

# Syntheses of Mesostructured Silica Films Containing Conjugated Polymers from Tetrahydrofuran–Water Solutions

S. Kirmayer,<sup>†</sup> E. Dovgolevsky,<sup>†</sup> M. Kalina,<sup>†</sup> E. Lakin,<sup>†</sup> S. Cadars,<sup>‡</sup> J. D. Epping,<sup>‡</sup>  
A. Fernández-Arteaga,<sup>§</sup> C. Rodríguez-Abreu,<sup>§</sup> B. F. Chmelka,<sup>‡</sup> and G. L. Frey<sup>\*†</sup>

Department of Materials Engineering, Technion - Israel Institute of Technology, Haifa 32000, Israel, Department of Chemical Engineering, University of California, Santa Barbara, California 93106, and Institut d'Investigacions Químiques i Ambientals de Barcelona, Consejo Superior de Investigaciones Científicas (IIQAB/CSIC), Jordi Girona, 18-26, 08034 Barcelona, Spain

Received December 6, 2007. Revised Manuscript Received February 5, 2008

Co-self-assembly of mesostructured silica films from solutions of tetrahydrofuran (THF) and water, silica precursor species, and structure-directing Pluronic P123 block-copolymer molecules is reported with and without conjugated polymer guest species. The solution-phase behavior of the ternary THF–water–P123 system guided the selection of nonequilibrium synthesis conditions that allowed highly ordered 2D hexagonal or lamellar mesostructured silica to be prepared. Dilute water molecules produced in situ by silica condensation were necessary and sufficient to promote P123 self-aggregation into micelles and ultimately liquid crystal-like inorganic–organic mesophases as the THF evaporated. Solid-state two-dimensional <sup>13</sup>C{<sup>1</sup>H} and <sup>29</sup>Si{<sup>1</sup>H} NMR characterization of the product film materials revealed highly mobile block copolymer components at room temperature and preferential interactions of poly(ethylene oxide) moieties with the silica framework at 260 K. Solution processing in THF permitted highly hydrophobic, high molecular weight, conjugated polymers to be directly coassembled within the mesostructured inorganic–organic host matrices during their formation. The incorporated conjugated polymers exhibited semiconducting properties and enhanced environmental photo-stability that may be exploited in electronic and optoelectronic devices.

## Introduction

Composite materials are designed to exploit beneficial properties of their individual components and to obtain desirable properties that are, in many cases, distinct or not possible to obtain from the separate constituent species. A promising class of composites is based on the incorporation of functional organic species into mesoscopically ordered inorganic matrices. These materials offer prospects for incorporating properties that can be adjusted, according to the interactions of the functional organic species with each other, with the organic structure-directing agents, and/or with the inorganic host. A wide range of metal oxides have been used to form continuous inorganic scaffolds,<sup>1,2</sup> among which silica is the most widely exploited, in part due to its facile processability. Organically functionalized mesoporous silicas have found applications in biotechnology,<sup>3</sup> catalysis,<sup>4,5</sup> separation and extraction processes,<sup>6,7</sup> energy conversion

applications,<sup>8,9</sup> and controlled release and drug delivery,<sup>10–12</sup> among others.

Mesostructured inorganic–oxide frameworks are conventionally synthesized by using aqueous sol–gel chemistry in the presence of structure-directing amphiphilic surfactant species. Under these conditions, hydrolysis and condensation of a network-forming inorganic precursor species, usually an inorganic alkoxide, occur in an aqueous solution.<sup>13</sup> Depending on the solution composition (e.g., pH and solvents) and synthesis conditions (e.g., temperature), different amphiphilic molecules, for example, low-molecular weight surfactants or block copolymers, can interact strongly with the inorganic precursor species and self-assemble into liquid-crystal-like mesophases.<sup>14,15</sup> When guest species, organic or otherwise, are also to be incorporated during self-

\* Corresponding author. E-mail: gitti@tx.technion.ac.il.

<sup>†</sup> Technion - Israel Institute of Technology.

<sup>‡</sup> University of California.

<sup>§</sup> Consejo Superior de Investigaciones Científicas.

- (1) Yang, P. D.; Zhao, D. Y.; Margolese, D. I.; Chmelka, B. F.; Stucky, G. D. *Chem. Mater.* **1999**, *11*, 2813.
- (2) Brezesinski, T.; Smarsly, B.; Iimura, K.; Grosso, D.; Boissiere, C.; Amenitsch, H.; Antonietti, M.; Sanchez, C. *Small* **2005**, *1*, 889.
- (3) Yan, X. X.; Deng, H. X.; Huang, X. H.; Lu, G. Q.; Qiao, S. Z.; Zhao, D. Y.; Yu, C. Z. *J. Non-Cryst. Solids* **2005**, *351*, 3209.
- (4) Nakajima, K.; Tomita, I.; Hara, M.; Hayashi, S.; Domen, K.; Kondo, J. N. *Catal. Today* **2006**, *116*, 151.
- (5) Feng, Y. F.; Yang, X. Y.; Di, Y.; Du, Y. C.; Zhang, Y. L.; Xiao, F. S. *J. Phys. Chem. B* **2006**, *110*, 14142.

(6) Tseng, H. E.; Liu, C. Y.; Chen, S. A. *Appl. Phys. Lett.* **2006**, *88*.

(7) McKinley, S. G.; Angelici, R. J. *Chem. Commun.* **2003**, 2620.

(8) Font, J.; de March, P.; Busque, F.; Casas, E.; Benitez, M.; Teruel, L.; Garcia, H. *J. Mater. Chem.* **2007**, *17*, 2336.

(9) Halla, J. D.; Mamak, M.; Williams, D. E.; Ozin, G. A. *Adv. Funct. Mater.* **2003**, *13*, 133.

(10) Nicole, L.; Boissiere, C.; Grosso, D.; Quach, A.; Sanchez, C. *J. Mater. Chem.* **2005**, *15*, 3598.

(11) Nguyen, T. D.; Leung, K. C. F.; Liong, M.; Pentecost, C. D.; Stoddart, J. F.; Zink, J. I. *Org. Lett.* **2006**, *8*, 3363.

(12) Balas, F.; Manzano, M.; Horcajada, P.; Vallet-Regi, M. *J. Am. Chem. Soc.* **2006**, *128*, 8116.

(13) Warren, W. L.; Lenahan, P. M.; Brinker, C. J.; Ashley, C. S.; Reed, S. T. *J. Electron. Mater.* **1990**, *19*, 425.

(14) Kresge, C. T.; Leonowicz, M. E.; Roth, W. J.; Vartuli, J. C.; Beck, J. S. *Nature* **1992**, *359*, 710.

(15) Zhao, D. Y.; Feng, J. L.; Huo, Q. S.; Melosh, N.; Fredrickson, G. H.; Chmelka, B. F.; Stucky, G. D. *Science* **1998**, *279*, 548.

assembly, they must be compatible with the aqueous sol-gel or surfactant components so that they do not macroscopically phase-separate from the synthesis mixture. For example, partially soluble dye molecules added to an aqueous silica-precursor solution in the presence of amphiphilic structure-directing agents have been shown to self-assemble into mesostructured silica/block-copolymer/dye composites with laser-like or optical limiting properties.<sup>16–27</sup> In polar solvents, occasionally with the addition of cosolvents, this has been used to advantage for a variety of polar organic dyes, including rhodamine 6G,<sup>18</sup> porphyrins,<sup>19,21</sup> spyropyrans and spirooxazines,<sup>16,22</sup> coumarin dyes,<sup>23</sup> fluorescein,<sup>24</sup> carbazole, and fluorene,<sup>25</sup> and other small chromophores<sup>26,27</sup> in mesostructured inorganic-organic matrices. However, while the use of polar solvents is suitable for coassembling polar or surfactant-dispersible organic species into nanocomposite host matrices, in most cases, these conditions are less suitable for incorporating nonpolar species and are entirely infeasible for highly hydrophobic guest molecules, such as most conjugated polymers.

One way to overcome the incompatibility of nonpolar or highly hydrophobic organic guest molecules in polar sol-gel solvents is to incorporate them into mesoporous hosts following removal of the surfactant species. Tolbert and co-workers have used this approach to incorporate hydrophobic conjugated polymers into calcined mesoporous silica after functionalizing the internal mesopore surfaces with grafted hydrophobic alkyl moieties.<sup>28,29</sup> In these and related studies,<sup>30,31</sup> moderately large (ca. 50 kDa) and flexible conjugated polymer molecules were infiltrated into the pores of mesostructured silica hosts. Alternatively, monomeric conjugated precursors can be incorporated into the voids of mesoporous silica, and subsequently *in situ* polymerized in

the presence of suitable catalysts. However, the steric limitations imposed by the pore dimensions and geometry lead to low-polymerization yields and prevent facile removal of residual catalyst, reaction byproducts, and unreacted monomers that can deleteriously influence the nanocomposite properties.

Another approach involves the coassembly of inorganic<sup>32</sup> or surfactant<sup>33–35</sup> precursor species that have been modified to include a covalently bound functional organic moiety. Coorganization of such modified precursors has been shown to yield mesostructured composite materials in which the functional moieties have been incorporated into the host matrices, provided solvent and surfactant compatibilities are maintained. A variation of the latter approach is to use functional oligomers or polymers as the hydrophobic segment of the amphiphilic molecules, either by grafting hydrophilic side chains or attaching a hydrophilic block.<sup>36–38</sup> In general, however, the use of specialty precursor or surfactant species tends to require expensive starting reagents and is still accompanied by similar solubility and mutual compatibility considerations as those discussed above. Consequently, to our knowledge until now, all of the approaches have relied on mesostructured silica or titania hosts prepared from aqueous or polar solvents into which organic functional agents were incorporated. This has required the use of organic agents that are soluble in polar solvents for directly coassembled systems or postsynthetic incorporation into hydrophobically modified mesopore channels.

A more general and versatile approach is to use nonpolar solvents, in conjunction with nonpolar organic guest species, under conditions where they can coassemble directly in the presence of structure-directing surfactant agents and mesostructure-forming inorganic frameworks. For example, mesostructured silica was prepared from a tetrahydrofuran (THF) precursor sol using poly(ethylene oxide)-*b*-polystyrene diblock copolymer surfactant species,<sup>39,40</sup> although without inclusion of guest species. Recently, the coassembly of highly hydrophobic conjugated polymer guest species into mesostructured composite films of silica/nonionic surfactants and their integration into optoelectronic devices have been demonstrated, though that study focused on device properties with little discussion of the underlying synthesis conditions or mechanisms.<sup>41</sup>

Here, we report a general method for the synthesis of mesostructured silica films from initially THF sols that permit

- (16) Scott, B. J.; Wirnsberger, G.; McGehee, M. D.; Chmelka, B. F.; Stucky, G. D. *Adv. Mater.* **2001**, *13*, 1231.
- (17) Wirnsberger, G.; Scott, B. J.; Chmelka, B. F.; Stucky, G. D. *Adv. Mater.* **2000**, *12*, 1450.
- (18) Yang, P. D.; Wirnsberger, G.; Huang, H. C.; Cordero, S. R.; McGehee, M. D.; Scott, B.; Deng, T.; Whitesides, G. M.; Chmelka, B. F.; Buratto, S. K.; Stucky, G. D. *Science* **2000**, *287*, 465.
- (19) Melosh, N. A.; Steinbeck, C. A.; Scott, B. J.; Hayward, R. C.; Davidson, P.; Stucky, G. D.; Chmelka, B. F. *J. Phys. Chem. B* **2004**, *108*, 11909.
- (20) Yagi, K.; Shibata, S.; Yano, T.; Yasumori, A.; Yamane, M.; Dunn, B. *J. Sol-Gel Sci. Technol.* **1995**, *4*, 67.
- (21) Steinbeck, C. A.; Ernst, M.; Meier, B. H.; Chmelka, B. F. *J. Phys. Chem. C* **2008**, *112*, 2565.
- (22) Andersson, P.; Robinson, N. D.; Berggren, M. *Synth. Met.* **2005**, *150*, 217.
- (23) Yamaguchi, A.; Amino, Y.; Shima, K.; Suzuki, S.; Yamashita, T.; Teramae, N. *J. Phys. Chem. B* **2006**, *110*, 3910.
- (24) Yao, Y. F.; Zhang, M. S.; Shi, J. X.; Gong, M. L.; Zhang, H. J.; Yang, Y. S. *Mater. Lett.* **2001**, *48*, 44.
- (25) Huang, M. H.; Kartono, F.; Dunn, B.; Zink, J. I. *Chem. Mater.* **2002**, *14*, 5153.
- (26) Prene, P.; Lancelle-Beltran, E.; Boscher, C.; Belleville, P.; Buvat, P.; Sanchez, C. *Adv. Mater.* **2006**, *18*, 2579.
- (27) Lu, Y. F.; Ganguli, R.; Drewien, C. A.; Anderson, M. T.; Brinker, C. J.; Gong, W. L.; Guo, Y. X.; Soyez, H.; Dunn, B.; Huang, M. H.; Zink, J. I. *Nature* **1997**, *389*, 364.
- (28) Nguyen, T. Q.; Wu, J. J.; Doan, V.; Schwartz, B. J.; Tolbert, S. H. *Science* **2000**, *652*, 288.
- (29) Nguyen, T. Q.; Wu, J.; Tolbert, S. H.; Schwartz, B. J. *Adv. Mater.* **2001**, *13*, 609.
- (30) Molenkamp, W. C.; Watanabe, M.; Miyata, H.; Tolbert, S. H. *J. Am. Chem. Soc.* **2004**, *126*, 4476.
- (31) Posudievsky, O. Y.; Telbiz, G. M.; Rossokhaty, V. K. *J. Mater. Chem.* **2006**, *16*, 2485.

- (32) Margolese, D.; Melero, J. A.; Christiansen, S. C.; Chmelka, B. F.; Stucky, G. D. *Chem. Mater.* **2000**, *12*, 2448.
- (33) Liu, N. G.; Chen, Z.; Dunphy, D. R.; Jiang, Y. B.; Assink, R. A.; Brinker, C. J. *Angew. Chem., Int. Ed.* **2003**, *42*, 1731.
- (34) Lu, Y. F.; Yang, Y.; Sellinger, A.; Lu, M. C.; Huang, J. M.; Fan, H. Y.; Haddad, R.; Lopez, G.; Burns, A. R.; Sasaki, D. Y.; Shelnutt, J.; Brinker, C. J. *Nature* **2001**, *410*, 913.
- (35) Peng, H. S.; Tang, J.; Pang, J. B.; Chen, D. Y.; Yang, L.; Ashbaugh, H. S.; Brinker, C. J.; Yang, Z. Z.; Lu, Y. F. *J. Am. Chem. Soc.* **2005**, *127*, 12782.
- (36) Hsieh, C. C.; Lin, K. F.; Chien, A. T. *Macromolecules* **2006**, *39*, 3043.
- (37) Tajima, K.; Li, L. S.; Stupp, S. I. *J. Am. Chem. Soc.* **2006**, *128*, 5488.
- (38) Bhongale, C. J.; Hsu, C. S. *Angew. Chem., Int. Ed.* **2006**, *45*, 1404.
- (39) Yu, K.; Hurd, A. J.; Eisenberg, A.; Brinker, C. J. *Langmuir* **2001**, *17*, 7961.
- (40) Yu, K.; Smarsly, B.; Brinker, C. J. *Adv. Funct. Mater.* **2003**, *13*, 47.
- (41) Dovgolevsky, E.; Kirmayer, S.; Lakin, E.; Yang, Y.; Brinker, C. J.; Frey, G. L. *J. Mater. Chem.* **2008**, *18*, 423.

highly hydrophobic guest species, such as conjugated polymers, to be directly coassembled within inorganic–organic host matrices. In particular, THF is shown to possess a favorable combination of properties that are compatible with the self-assembly, cross-linking, and processing of nanocomposite silica materials. Key properties of THF are its high volatility under ambient synthesis conditions, low viscosity for film processing, and high solution miscibilities for the poly(ethylene oxide)–poly(propylene oxide)–poly(ethylene oxide) (PEO–PPO–PEO) triblock copolymer surfactants, alkoxide inorganic precursors, hydrophobic conjugated polymer guest molecules, and water. Detailed understanding of the phase behavior of the ternary THF–water–P123 system and of the molecular compositions and structures of the mesostructured silica products have been obtained from birefringence, SAXS, and multidimensional solid-state NMR measurements. By using the resulting macroscopic and molecular-level insights, highly ordered lamellar or hexagonal nanocomposite silica films can be obtained from THF sols, depending on the relative concentrations of surfactant, water, and silica source. Highly hydrophobic conjugated polymer guest species with high molecular weights (ca. 200 kDa) and/or with molecularly rigid structures are shown to be incorporated during synthesis and processing of mesostructurally ordered nanocomposite thin films. The incorporated conjugated polymers are furthermore shown to have stable semiconducting properties that may be useful in electronic and optoelectronic applications.

### Experimental Section

**Materials.** Analytical grade THF (AR, BioLab, Israel), tetraethoxysilane (TEOS 98% GC, Aldrich, Germany), and HCl 0.07 M (Carlo Erba, Italy) were used as-received. The structure-directing surfactant, Pluronic P123 ( $M_n = 5750$  g/mol)  $\text{EO}_{20}\text{PO}_{70}\text{EO}_{20}$ , where “EO” represents the ethylene oxide monomer segments and “PO” the propylene oxide segments of which the poly(ethylene oxide) (PEO) and poly(propylene oxide) (PPO) blocks are comprised, was received as a gift from BASF, U.S.A., and used as-received. The two conjugated polymers used in this study were purchased from ADS, Canada, and used as-received: poly[2-methoxy-5-(2'-ethylhexyloxy)-1,4-phenylene vinylene] (MEH-PPV,  $M_w = 200$  kDa), and poly(9,9'-dioctylfluorene) (PFO,  $M_w = 74$  kDa).

**Precursor Solutions.** A prehydrolyzed silica sol was prepared by mixing 75 mL of THF, 15 mL of TEOS, and 6 mL of HCl (0.07 M), followed by sonication in an ultrasonic bath for 1 h. Variable amounts of P123, in the range of 0–0.8 g, were dissolved in 1.5 mL of the THF–silica sol to obtain a surfactant–sol solution. Separately, 7.5 mg of MEH-PPV, or 5 mg of PFO, were fully dissolved in 2.5 mL of THF, occasionally using mild heating conditions (up to 333 K) and stirring. Prior to film deposition, 2.2 mL of the conjugated polymer solutions (filtered through 0.45  $\mu\text{m}$  PTFE membrane) or 2.2 mL of pure THF (for the deposition of films without conjugated-polymer guest species) were added to the surfactant–sol solution. The molar ratios in the final precursor solutions were 40.5 THF:1.0 TEOS:4.8  $\text{H}_2\text{O}$ :0.006 HCl: $x$  Pluronic: $y$  conjugated polymer, where  $0.009 \leq x \leq 0.132$  and  $y = 0$  or  $4.3 \times 10^{-5}$  for MEH-PPV or  $7.1 \times 10^{-5}$  for PFO.

**Film Deposition.** Nanocomposite thin films were prepared by dip-coating  $12 \times 25$  mm<sup>2</sup> glass microscope slides or polyimide films at a rate of 2 mm/s from the final precursor solutions (with or without conjugated polymer guest species), at 295 K and high relative humidity (>50%). The film thickness, 200–400 nm

(measured with a profiler Alpha-step 200, Tencor), depends on the surfactant concentration in the precursor solution, which affects its viscosity. Regardless of the type or concentrations of the conjugated polymer species or P123 concentration, all films dip-coated from the THF precursor solutions were transparent (>80%) and adhered well to the substrates. Free-standing films were separately prepared by slow solvent evaporation from the final precursor solutions in a Petri dish under a THF atmosphere. All films were stored in a glovebox (water and oxygen <10 ppm) after preparation, prior to subsequent characterization measurements.

Conjugated polymer loadings were estimated by dissolving freshly deposited films in known small amounts of THF under vigorous stirring. The concentration of the conjugated polymer in the solution was determined by optical absorption spectroscopy. The substrate was weighed prior to and after film removal to estimate total film weight from which conjugated polymer loadings of 0.5–1 wt % were calculated.

**Characterization.** The THF–water–P123 phase diagram was determined by preparing 75 samples with varied compositions in glass tubes. To avoid solvent evaporation, the mixtures were frozen in liquid nitrogen and quickly flame sealed. Mixing was accomplished by repeated centrifugation through the narrow constrictions made in the tubes. Before observations, the samples were kept in a freezer for 24 h and then allowed to equilibrate in a thermostatic bath at 298 K for several days. The phases were identified by eye (turbidity, viscosity), using polarizers (birefringence), and by video-enhanced optical microscope (characteristic textures). In some cases, the solvent-penetration-scan method (or inversely, partial evaporation) was used to identify phases by microscopy in a narrow range of compositions. To identify the liquid crystal phases present, SAXS measurements were performed in an MBraun instrument equipped with a Siemens Kristalloflex 760 (K-760) generator, operating at 50 kV and between 10 and 30 mA, and a Kratky Hecus MBraun-Graz camera. The collimator was a slit window, and the scattering was detected with a linear position-sensitive detector OED-50M. The temperature controller was an AP Paar K-PR Peltier device.

Light scattering measurements were conducted on THF–water–P123 mixtures that were homogenized in an ultrasonic bath, left to equilibrate overnight, and filtered immediately prior to measurement to remove dust particles (Micropore 0.45  $\mu\text{m}$  pressure filtration). The solution vials were then immersed in a glass reservoir containing decalin at 298 K as the index matching fluid. The static light scattering measurements were performed using a BI-200SM Research Goniometer System (Brookhaven Instruments Corp.) with a Compass 415 M solid-state laser (Coherent) generating monochromatic green light of 532 nm at a 90° configuration.

One-dimensional (1D) X-ray diffraction (XRD) measurements were performed on a Bede D<sup>3</sup> X-ray diffractometer equipped with an 18 kW Rigaku rotating anode generator at  $\theta$ – $2\theta$  scan mode in reflection geometry. A highly monochromatized Cu  $K_{\alpha 1}$  line with  $\lambda = 1.5406$  Å was selected from the primary X-ray beam by means of two channel-cut (220) Si crystals. Small-angle X-ray scattering (SAXS) measurements were performed using a small-angle diffractometer (Bruker Nanostar, KFF CU 2 K-90) with Cu  $K_{\alpha}$  radiation with  $\lambda = 1.542$  Å. Pinhole collimation yielding a beam 100  $\mu\text{m}$  in diameter and a  $10 \times 10$  cm<sup>2</sup> two-dimensional (2D) position-sensitive wire detector positioned 64.3 cm behind the sample were used. The patterns were recorded using an acceleration voltage of 40 kV and acceleration current of 20 mA. The polyimide substrates were vertically located in the SAXS diffractometer, and patterns were recorded in transmission mode with fixed incidence angle  $\alpha$  (the angle between the incident beam and the sample surface) of approximately 2°. This configuration, referred to as “glancing incidence”, mimics the “grazing incidence” technique

where the X-ray beam is incident at nearly the critical angle.<sup>42</sup> The 2D SAXS “glancing incidence” scattering geometry shows diffracted intensity exclusively out of the film plane.

Transmission electron microscopy (TEM) measurements were performed using a FEI Tecnai T12 G<sup>2</sup> transmission electron microscope operating at 120 keV. Optical absorption spectra were measured using a Varian Cary 100 Scan UV–vis spectrophotometer. A Varian Cary Eclipse spectrofluorometer was used to measure the photoluminescence (PL) spectra, with 495 and 380 nm excitation wavelengths for the MEH-PPV and PFO, respectively.

Solid-state <sup>13</sup>C{<sup>1</sup>H} and <sup>29</sup>Si{<sup>1</sup>H} HETCOR NMR experiments were conducted on a Bruker DMX-300 spectrometer with a wide-bore 7.0 T superconducting magnet operating at <sup>1</sup>H, <sup>13</sup>C, and <sup>29</sup>Si Larmor frequencies of 300.1, 75.5, and 59.6 MHz, respectively. The experiments were carried out at room temperature under magic-angle-spinning (MAS) conditions (12.5 kHz) using a double-resonance probehead, on powders prepared from free-standing films. (SAXS measurements corroborated that free-standing and dip-coated films prepared from identical precursor solutions yielded materials with the same mesostructural ordering.) Cross-polarization for transferring magnetization from the abundant protons to <sup>13</sup>C or <sup>29</sup>Si nuclei was achieved by an adiabatic passage through the Hartmann–Hahn conditions.<sup>43</sup> Heteronuclear <sup>1</sup>H decoupling was applied during acquisition at the <sup>1</sup>H nutation frequency of 80 kHz, using SPINAL64.<sup>44</sup> Quadrature detection in the indirect dimension was achieved using the TPPI procedure.<sup>45</sup> For the 2D <sup>13</sup>C{<sup>1</sup>H} HETCOR spectrum, a contact time of 3 ms was used with 48 transients for each of the 256 *t*<sub>1</sub> increments and a recycle delay of 2.5 s (total duration of 3 h). The contour levels of the 2D <sup>13</sup>C{<sup>1</sup>H} HETCOR spectrum correspond to 10, 25, 40, 55, 70, and 85% of the maximum signal intensity. For the <sup>29</sup>Si{<sup>1</sup>H} HETCOR spectrum, a contact time of 8 ms, using 384 transients for each of the 48 *t*<sub>1</sub> increments, and a recycle delay of 2.5 s (13 h total) were used. The contour levels of the 2D <sup>29</sup>Si{<sup>1</sup>H} HETCOR spectrum correspond to 8, 18, 28, ..., 88, and 98% of the maximum signal intensity.

Low-temperature (ca. 260 K) 2D <sup>29</sup>Si{<sup>1</sup>H} HETCOR NMR experiments were recorded at 11.74 T on a Bruker AVANCE II wide-bore spectrometer operating at frequencies of 500.24 MHz for <sup>1</sup>H, 125.79 MHz for <sup>13</sup>C, and 99.39 MHz for <sup>29</sup>Si. HETCOR NMR experiments were carried out under MAS conditions at 12.5 kHz using a double resonance probehead. Adiabatic cross-polarization with contact times of 6 or 1 ms were employed to transfer the magnetization from the protons to <sup>29</sup>Si nuclei.<sup>43</sup> Strong <sup>1</sup>H–<sup>1</sup>H dipolar couplings may be partially, but are often incompletely, averaged even under fast MAS conditions, leading to peak broadening and deterioration in spectral resolution. Such difficulties may be overcome or mitigated by the use of multiple-pulse sequences for homonuclear <sup>1</sup>H decoupling, which can lead to significantly improved resolution.<sup>46–50</sup> The incorporation of homonuclear-decoupling pulse sequences into 2D HETCOR NMR

experiments similarly yield enhanced resolution of signals in the indirectly detected <sup>1</sup>H dimension. At 260 K, strong residual dipolar couplings between the abundant protons were partially suppressed during the *t*<sub>1</sub> evolution period by using the eDUMBO-1<sub>22</sub> homonuclear <sup>1</sup>H decoupling sequence<sup>48,49</sup> at a nutation frequency of 100 kHz. The indirect dimension was recorded using 192 *t*<sub>1</sub> increments, with the States method for quadrature detection.<sup>51</sup> A “magic pre-pulse” of 1.4 μs (ca. 50° at 100 kHz) was employed to flip the <sup>1</sup>H magnetization back to the transverse plane, after nutation around the effective RF field of the homonuclear decoupling, which is tilted at the magic angle with respect to the static field.<sup>46</sup> Scaling factors of 0.55 resulting from homonuclear decoupling in the indirect dimension were calculated from separate <sup>1</sup>H{<sup>1</sup>H} spin-diffusion experiments with homonuclear decoupling applied under similar conditions during the *t*<sub>1</sub> evolution period and using a very short (5 μs) mixing time to observe only the diagonal peaks.

Chemical shifts were referenced relative to neat TMS (0.00 ppm), using tetrakis-methylsilane as an external secondary reference (with <sup>29</sup>Si, <sup>13</sup>C, and <sup>1</sup>H chemical shifts of –9.84, 3.52, and 0.25 ppm relative to TMS, respectively).<sup>52</sup> Assignment of the <sup>13</sup>C NMR peaks of the P123 block copolymer were obtained from separate solution-state <sup>13</sup>C NMR measurements conducted on 15 wt % P123 in deuterated THF (not shown), including single-pulse <sup>13</sup>C NMR and a series of DEPT experiments for spectral editing.

## Results and Discussion

**Mesostructured Silica Formed from THF–Water Solutions.** The deposition of mesostructured silica films from aqueous/ethanol sols is a result of two concurrent processes: the self-organization of surfactant species into liquid-crystal-like mesophase domains, and the polymerization and cross-linking of silica.<sup>53</sup> These processes are driven by the increasing concentrations of the surfactant and the hydrolyzed silica species during solvent evaporation. In this study, the usual aqueous/ethanol-based sol was replaced with a THF sol, in view of incorporating highly hydrophobic species, such as conjugated polymers, into the mesostructured silica matrix *during* its formation. THF was selected as the solvent, because it solubilizes hydrophobic conjugated polymer molecules, the block copolymer species, and the silica precursor species, and because it is highly volatile and evaporates rapidly at room temperature.<sup>41</sup>

Little is known about how mesostructural order develops in multicomponent inorganic–organic systems prepared in the presence of nonaqueous or nonalcoholic solvents. Accompanying self-assembly of the components is often further complicated by nonequilibrium processes, such as solvent evaporation and inorganic cross-linking. In part, this is because the phase behavior of even simple ternary equilibrium systems, such as THF–water–P123 (or other Pluronic-type surfactants), has not been available in the literature to guide more complicated multicomponent and nonequilibrium sol–gel-based material syntheses. Therefore, to develop a protocol for the deposition of mesostructured silica from THF, it was first necessary to investigate the phase behavior of the surfactant, Pluronic P123 in this case, in THF (without

(42) Hayward, R. C.; Alberius, P. C. A.; Kramer, E. J.; Chmelka, B. F. *Langmuir* **2004**, *20*, 5998.

(43) Hediger, S.; Meier, B. H.; Kurrer, N. D.; Bodenhausen, G.; Ernst, R. R. *Chem. Phys. Lett.* **1994**, *223*, 283.

(44) Fung, B. M.; Khitrin, A. K.; Ermolaev, K. *J. Magn. Reson.* **2000**, *142*, 97.

(45) Marion, D.; Wuthrich, K. *Biochem. Biophys. Res. Commun.* **1983**, *113*, 967.

(46) Lee, M.; Goldburg, W. I. *Phys. Rev.* **1965**, *140*, 1261.

(47) Vinogradov, E.; Madhu, P. K.; Vega, S. *Chem. Phys. Lett.* **1999**, *314*, 443.

(48) Sakellariou, D.; Lesage, A.; Hodgkinson, P.; Emsley, L. *Chem. Phys. Lett.* **2000**, *319*, 253.

(49) Elena, B.; de Paepe, G.; Emsley, L. *Chem. Phys. Lett.* **2004**, *398*, 532.

(50) Bielecki, A.; Kolbert, A. C.; de Groot, H. J. M.; Griffin, R. G.; Levitt, M. H. *Adv. Magn. Reson.* **1990**, *14*, 111.

(51) States, D. J.; Haberkorn, R. A.; Ruben, D. *J. Magn. Reson.* **1982**, *48*, 286.

(52) Hayashi, S.; Hayamizu, K. *Bull. Chem. Soc. Jpn.* **1991**, *64*, 685.

(53) Soler-Illia, G. J. A. A.; Innocenzi, P. *Chem. Eur. J.* **2006**, *12*, 4478.

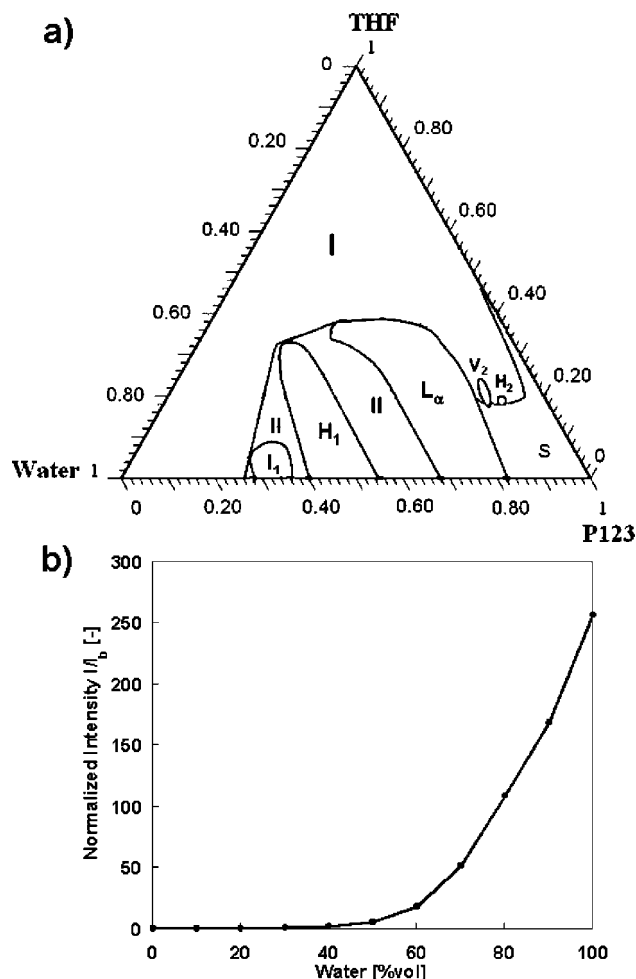


**Figure 1.** (a) The ternary phase diagram of THF–water–P123 at 298 K (the concentrations are expressed in weight percent).  $I_1$  is a normal micellar cubic liquid crystal phase,  $H_1$  is a normal hexagonal phase,  $L_\alpha$  is a lamellar phase,  $V_2$  is a reverse bicontinuous cubic phase, and  $H_2$  is a reverse hexagonal phase.  $II$  is a multiphase liquid crystal region, and  $S$  is a multiphase region containing solid and liquid crystal phases.  $I$  is an isotropic single-phase region. (b) Static light scattering from ternary THF–water–P123 solutions containing a fixed concentration of 10 mM surfactant and varied water volumetric fraction in the THF–water mixture.  $I_0$  is the background scattering intensity.

the presence of the silica precursor and conjugated polymer guest species).

The high solubility and nonselectivity of THF toward the hydrophobic and hydrophilic blocks of P123 at room temperature prevent the self-organization of P123 into micellar aggregates in THF. However, beyond the solubility limit of P123 in THF,  $\sim 52$  wt %, P123 precipitates as a solid, as evident from the right axis of the ternary THF–water–P123 phase diagram at 298 K shown in Figure 1a. The ternary phase diagram also shows that addition of water to a solution of P123 in THF initially results in an isotropic solution, which contains both monomeric P123 and micellar solutions (denoted as  $I$  in the phase diagram shown in Figure 1a). Increasing the water and/or P123 contents in the mixture leads to the evolution of liquid crystal phases, including micellar cubic ( $I_1$ ), hexagonal ( $H_1$ ), and lamellar ( $L_\alpha$ ) mesophases (Figure 1a). At 298 K, no liquid crystal phase is found above approximately 40 wt % of THF in this system, suggesting that a minimum amount of water is

required to induce a solvophobic effect in P123 molecules (specifically the PPO chains), which accounts for self-organization in the present case. It is interesting to compare the THF–water–P123 phase diagram presented here (Figure 1a) with that of ethanol–water–P123, because ethanol is commonly used in syntheses of mesostructured silica, either as a cosolvent or as a hydrolysis byproduct. According to the ethanol–water–P123 phase diagram,<sup>54</sup> no liquid crystal phase is formed at 295 K above approximately 25 wt % ethanol, significantly lower than in THF. This indicates that P123 self-organization is favored in THF–water solutions, compared to ethanol–water mixtures.

Notably, for the ternary THF–water–P123 system, a bicontinuous cubic liquid crystal phase ( $V_2$ ) and a reverse hexagonal phase ( $H_2$ ) were identified in a very narrow composition range at high P123 concentrations. The  $V_2$  and  $H_2$  phases are not found in binary water–P123 or ethanol–P123 solutions nor in the reported ternary ethanol–water–P123 system.<sup>54</sup> The formation of such phases in the THF–water–P123 system suggests that THF affects the interfacial curvature of P123 aggregates and associated molecular packing constraints in a particular way. In fact, as can be deduced from Figure 1a, adding THF to water–P123 mixtures can induce  $I_1$ – $H_1$  phase changes (at low P123:water ratios) or  $H_1$ – $L_\alpha$  transitions (at high P123:water ratios). These phase changes are consistent with a decrease in aggregate curvature in the presence of THF, which is further corroborated by the formation of reverse  $V_2$  and  $H_2$  liquid crystals at high P123 concentrations. A more detailed study on the effect of THF on the self-organization of PEO–PPO–PEO systems will be reported elsewhere.

The dependence of P123 self-organization on the availability of water molecules in an isotropic mixture of P123, water, and THF is reflected in light scattering measurements, as shown in Figure 1b. The scattering intensity from a solution of 10 mM P123 in a THF–water mixture, with water volume fraction less than 40%, is at the level of the background. Under these conditions, the P123 is solubilized in the solvent, in agreement with the phase diagram (Figure 1a). Increasing the water fraction above 40 vol % leads to a dramatic increase in the light-scattering intensity, associated with the self-assembly of the triblock-copolymer surfactant into micelles, that then concentrate and eventually rearrange into liquid-crystal-like mesophases. Self-assembly of P123 in the nonselective THF solvent thus appears to rely on the presence of sufficient water molecules, which are expected to interact preferentially with the hydrophilic PEO blocks of P123 to promote mesophase formation.

The water concentration required to initiate P123 self-association into micelle-like aggregates will depend crucially on the composition of the surfactant sol solution, namely, the concentrations of the silica precursor, surfactant, and solvent species present. To identify the conditions for the formation of silica mesophases from THF–water–P123

(54) (a) Soni, S. S.; Brotons, G.; Bellour, M.; Narayanan, T.; Gibaud, A. *J. Phys. Chem. B* **2006**, *110*, 15157. (b) Melosh, N. A.; Lipic, P.; Bates, F. S.; Wudl, F.; Stucky, G. D.; Fredrickson, G. H.; Chmelka, B. F. *Macromolecules* **1999**, *32*, 4332.

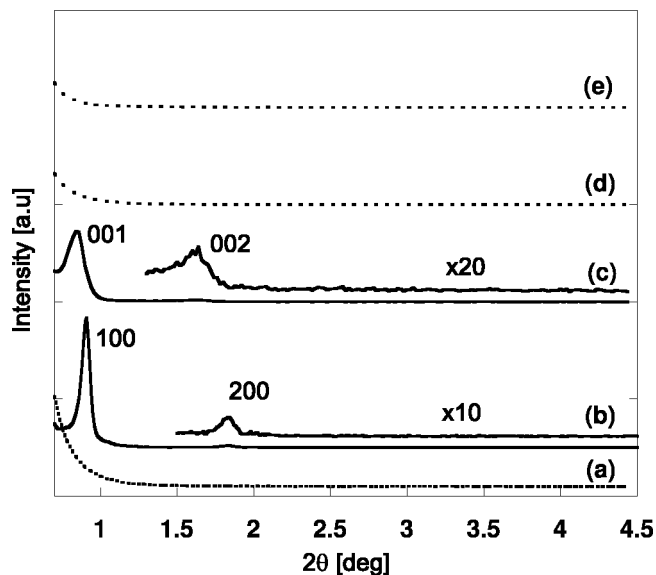


**Figure 2.** 1D SAXS patterns of silica films deposited from THF precursor sols with variable concentrations of P123. TEOS:P123 molar ratios are (a) 1:0, (b) 1:0.017, (c) 1:0.033, (d) 1:0.066, and (e) 1:0.132.

mixtures, films were dip-coated from THF precursor solutions with TEOS:P123 molar ratios ranging between 1:0 and 1:0.132 and subsequently analyzed by 1D SAXS (Figure 2). Films deposited from solutions with TEOS:P123 molar ratios of 1:0.017 and 1:0.033 gave well-resolved reflections, indicating the presence of an ordered, self-organized silica mesostructure. Reflections are observed in both patterns (Figure 2b,c) at  $2\theta$  angles of  $0.91^\circ$  and  $1.82^\circ$  for the films deposited from the 1:0.017 TEOS:P123 molar ratio of THF sol, corresponding to  $d$ -spacings of 9.7 and 4.9 nm, respectively. Similarly, for the film deposited from the THF sol with a 1:0.033 TEOS:P123 molar ratio, reflections at  $0.80^\circ$  and  $1.60^\circ$  were observed, corresponding to  $d$ -spacings of 11.0 and 5.5 nm. The absence of reflections in the 1D SAXS patterns of films deposited from precursor solutions with TEOS:P123 molar ratios with P123 contents either above 1:0.05 or below 1:0.013 (Figure 2 a,d,e) reveals that no mesostructural ordering occurs for these compositions.

The presence of a 2D hexagonal mesostructure, with arrays of cylinders aligned parallel to the substrate, is identified by 2D-SAXS and TEM measurements shown in Figure 3a for films deposited from precursor solutions with a TEOS:P123 molar ratio of 1:0.017. The 2D glancing-incidence SAXS (GISAXS) pattern shows sharp, intense  $\langle 100 \rangle$  reflections normal to the film plane and weaker  $\langle \bar{1}10 \rangle$  and  $\langle 010 \rangle$  reflections. This pattern reflects a highly regular 2D hexagonal structure with a  $d$ -spacing of 9 nm for the  $\langle 100 \rangle$  planes, in good agreement with the 1D X-ray results, and indicates orientational ordering of the cylinders in the plane of the substrate. The fingerprint-like pattern in the TEM image shows the cylinder arrays from the  $\langle 100 \rangle$  plane with a periodic spacing of approximately 9 nm, corroborating the parameters determined by the X-ray measurements.

A lamellar mesophase was found for the silica film deposited from a THF sol with TEOS:P123 molar ratio of 1:0.033. Figure 3b shows a 2D-SAXS pattern with two strong and exclusively out-of-the-film-plane (see Experimental

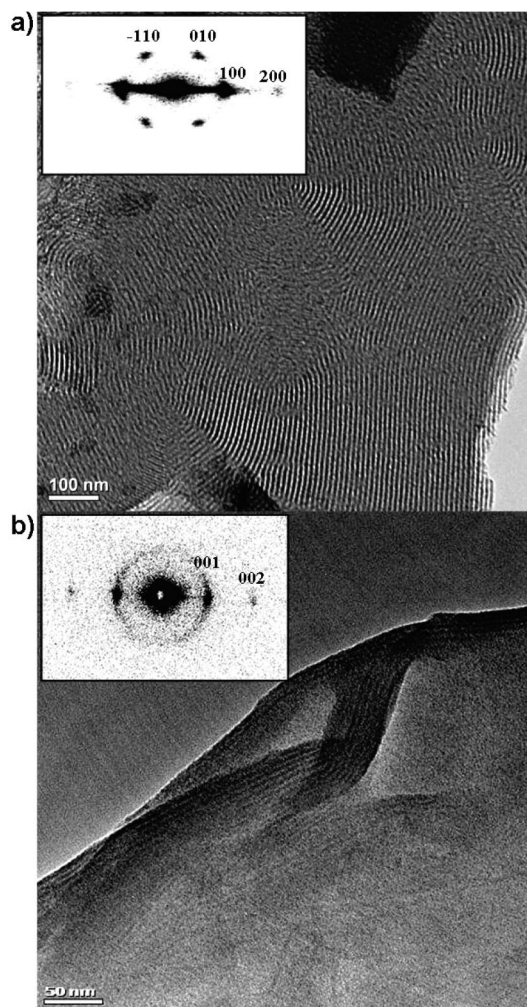


**Figure 3.** TEM images and glancing-incidence 2D-SAXS patterns (insets) of silica films deposited from THF sols with TEOS:P123 molar ratios of (a) 1:0.017 and (b) 1:0.033.

Section) reflections, indexed as  $\langle 001 \rangle$  and  $\langle 002 \rangle$  reflections of a lamellar structure aligned parallel to the substrate. The TEM image shows a top view of a silica domain, with features typical of a lamellar mesostructure only at the edges. Periodic spacings of approximately 5 nm, about half the  $d$ -spacing determined by the SAXS measurement, indicate that the layers are observed as a diagonal cross-section of the lamellar structure.

The surfactant and silica precursor species co-assemble in the sols as the THF evaporates during film processing, leading to the formation of the hexagonal and lamellar mesophases. While the transient nonequilibrium self-assembly process(es) are difficult to follow at a molecular level during film deposition, interactions among the numerous components are reflected in the interfacial compositions of the resulting nanocomposite products. In particular, the local compositions and structures, notably the proximities of different molecular species, at heterogeneous interfaces in the nanocomposites can be established by powerful solid-state 2D NMR techniques.

For example, 2D  $^{13}\text{C}\{^1\text{H}\}$  and  $^{29}\text{Si}\{^1\text{H}\}$  heteronuclear chemical shift correlation (HETCOR) NMR measurements unambiguously establish the molecular proximities of dif-

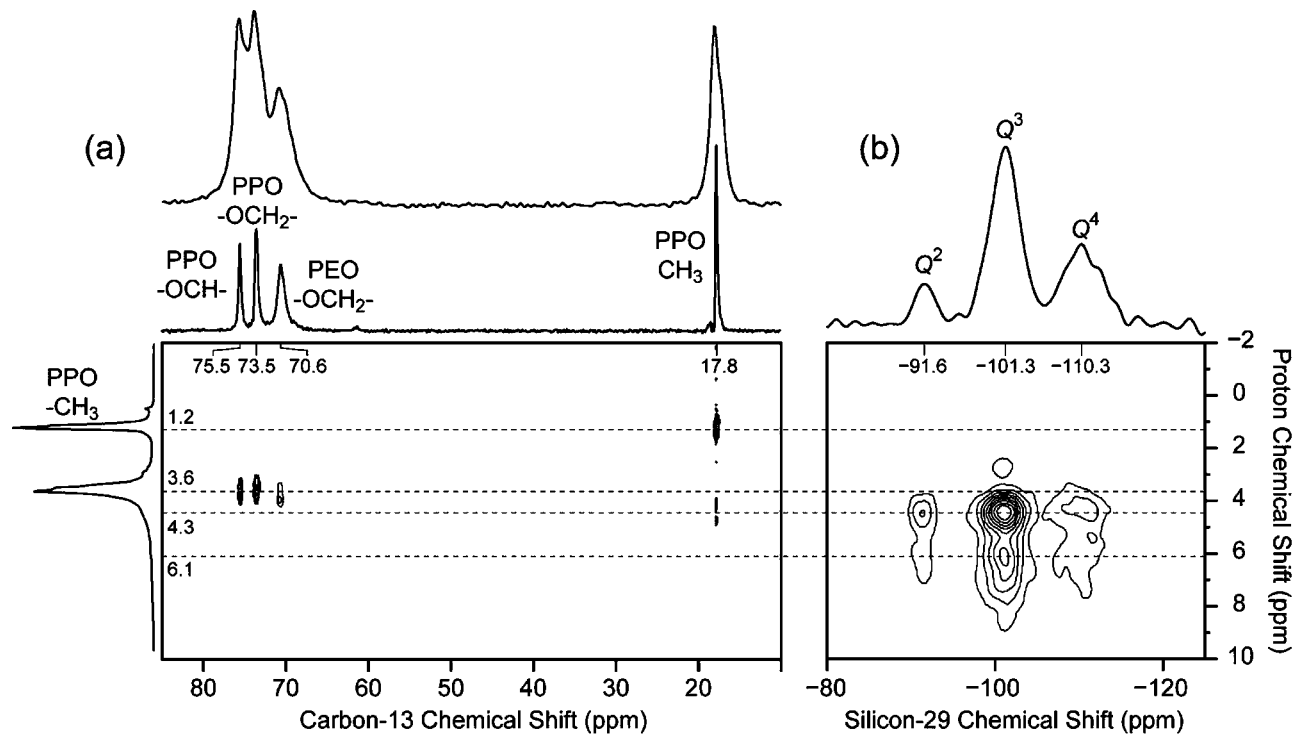


**Figure 4.** (a) Room-temperature 2D  $^{13}\text{C}\{^1\text{H}\}$  HETCOR spectrum of a powder prepared from a hexagonally mesostructured silica-P123 film (the same material used in Figure 2b and 3a). A single-pulse 1D  $^1\text{H}$  MAS spectrum and a 1D  $^{13}\text{C}\{^1\text{H}\}$  CP-MAS spectrum are shown along their corresponding axes. The uppermost 1D single-pulse  $^{13}\text{C}$  spectrum was recorded at room temperature under static conditions, with 1024 transients and using a recycle delay of 60 s. (b) Room-temperature  $^{29}\text{Si}\{^1\text{H}\}$  HETCOR spectrum of the same sample shown in (a). A single-pulse  $^{29}\text{Si}$  MAS spectrum recorded under identical conditions with a recycle delay of 100 s and 256 transients is shown along its corresponding axis. The proton axis corresponds to that in (a).

ferent PEO and PPO  $^1\text{H}$  and  $^{13}\text{C}$  moieties in the PEO-PPO-PEO copolymer blocks to each other and to the mesostructured silica framework. The solid-state 2D  $^{13}\text{C}\{^1\text{H}\}$  HETCOR spectrum acquired at room temperature for a powder sample prepared from hexagonal mesostructured silica-P123 films cast from THF solutions (without hydrophobic guest species) is shown in Figure 4a. A single-pulse 1D  $^1\text{H}$  MAS spectrum and 1D  $^{13}\text{C}\{^1\text{H}\}$  CP-MAS spectrum are shown along their corresponding axes, along with a 1D single-pulse  $^{13}\text{C}$  spectrum recorded at room temperature under static (non-spinning) conditions. All of the 1D spectra show well resolved peaks that correspond to  $^1\text{H}$  and  $^{13}\text{C}$  signals associated with the P123 triblock-copolymer species. Their assignments are unambiguously established by the 2D  $^{13}\text{C}\{^1\text{H}\}$  HETCOR spectrum, which shows numerous intensity correlations: between the signal at 1.2 ppm in the  $^1\text{H}$  dimension and 17.8 ppm in the  $^{13}\text{C}$  dimension, which is associated with the  $-\text{CH}_3$  groups of the PPO blocks; between the signal at 3.6 ppm in the  $^1\text{H}$  dimension and the two signals at 73.5 and 75.5 ppm in the  $^{13}\text{C}$  dimension, which are associated with the  $-\text{OCH}_2-$  and  $-\text{OCH}-$  groups, respectively, of the PPO blocks; and between the signal at 3.7 ppm in the  $^1\text{H}$  dimension and the signal at 70.6 ppm in the  $^{13}\text{C}$  dimension, which is associated with the  $-\text{OCH}_2-$  groups of the PEO blocks.

These 2D  $^{13}\text{C}\{^1\text{H}\}$  correlations and the 1D spectra are consistent with those observed by Melosh et al. for hexagonal mesostructured silica-F127 monoliths prepared from ethanolic solutions<sup>54b</sup> but differ in that all of the 1D  $^1\text{H}$  and  $^{13}\text{C}$  MAS peaks and 2D intensity correlations are much narrower in the otherwise similar nanocomposites prepared from THF

solutions. The narrow signals under MAS conditions reflect uniform environments that could be either due to high degrees of local solid-state order (e.g., crystallinity) or due to high molecular mobilities of the triblock copolymer segments that would average different local environments. These two possibilities are distinguished by the single-pulse (upper)  $^{13}\text{C}$  NMR spectrum acquired under static, but otherwise identical, conditions: resolved (albeit partially broadened) signals are observed even under non-MAS conditions, which confirms the highly mobile characters of both the PPO and the PEO moieties in the hexagonally mesostructured silica-P123 composites at ambient temperature. This indicates a higher degree of local separation of the structure-directing triblock-copolymer moieties from the glass-like silica framework, when the nanocomposite films are prepared from THF, as compared to ethanolic, precursor solutions.

Additional and corroborative molecular insights are provided by 2D  $^{29}\text{Si}\{^1\text{H}\}$  HETCOR measurements that directly probe interactions between hydrogen-containing moieties and the silica frameworks in the nanocomposite films. A 2D  $^{29}\text{Si}\{^1\text{H}\}$  HETCOR spectrum and accompanying single-pulse 1D  $^{29}\text{Si}$  MAS spectrum were acquired at room temperature for the same nanocomposite sample as above and are shown in Figure 4b. In the 2D  $^{29}\text{Si}\{^1\text{H}\}$  HETCOR spectrum, strong correlated signal intensity is observed between the broad but resolved peaks associated with the  $Q^2$ ,  $Q^3$ , and  $Q^4$  silica species at -91.6, -101.3, and -110.3 ppm, respectively,<sup>55</sup> in the  $^{29}\text{Si}$  dimension and peaks at 4.3 and 6.1 ppm in the  $^1\text{H}$  dimension, the latter of which are attributed to adsorbed water and hydrogen-bonded water, respectively, at or near frame-

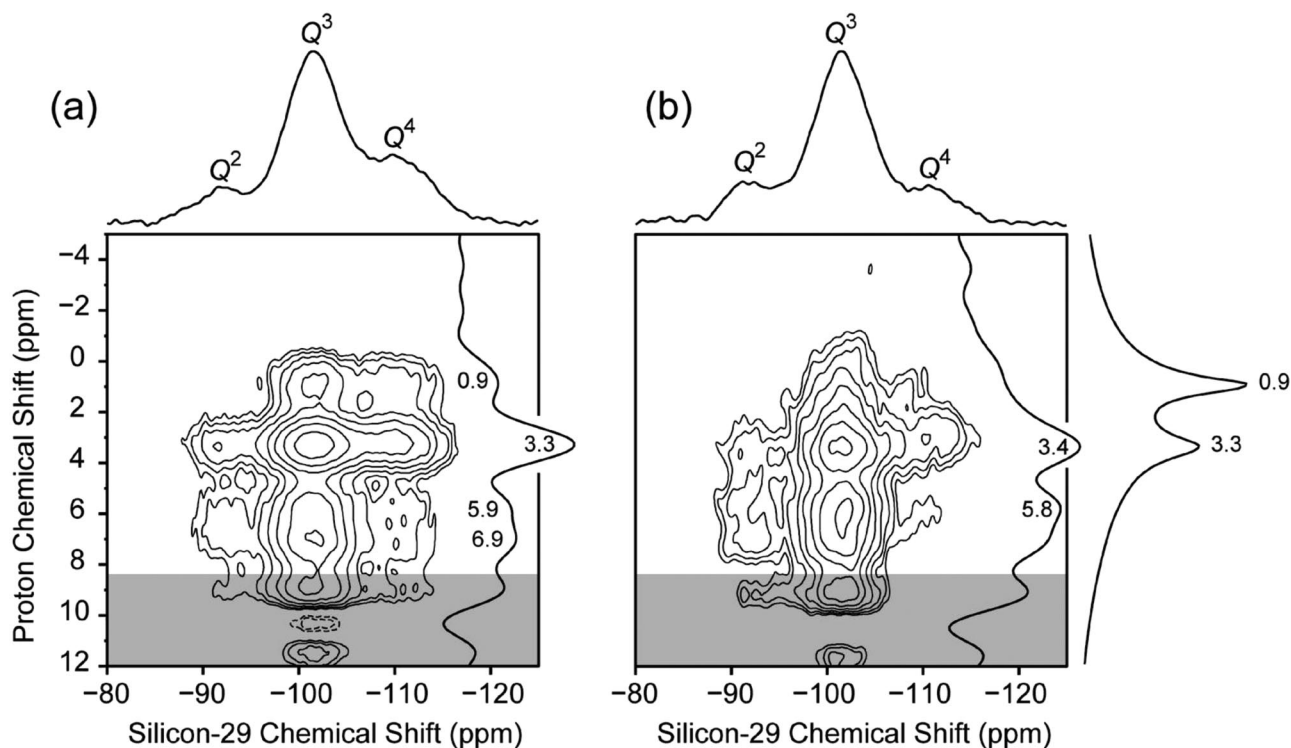


**Figure 5.** Low-temperature (ca. 260 K)  $^{29}\text{Si}\{^1\text{H}\}$  HETCOR spectra of the same hexagonal mesostructured silica films as shown in Figure 4 recorded at 12.5 kHz using CP contact times of (a) 6 ms and (b) 1 ms, with homonuclear  $^1\text{H}$  decoupling (DUMBO-1<sub>22</sub>) in the indirect dimension. 1D  $^{29}\text{Si}\{^1\text{H}\}$  CP-MAS spectra shown along the horizontal  $^{29}\text{Si}$  axes were recorded using 512 transients under identical conditions as used in the 2D HETCOR experiments. 1D projections onto the  $^1\text{H}$  axes are shown to the right of each 2D spectrum, and a quantitative 1D single-pulse  $^1\text{H}$  MAS spectrum recorded at approximately 260 K is shown along the vertical axis at the far right. The grey regions indicate artifacts due to homonuclear decoupling in the indirect dimension. The contour levels in (a) correspond to 8, 11, 21, 29, 40, 57, and 79% of the maximum signal intensity and in (b) to 15, 20, 25, 33, 43, 72, and 94%.

work silanol sites. Notably, at room temperature, *no* intensity correlations are observed between any of the  $^{29}\text{Si}$  framework sites and the  $^1\text{H}$  signals associated with the structure-directing P123 triblock copolymer species, even though a long 8-ms contact time was used to promote interactions among weakly dipole-dipole-coupled  $^{29}\text{Si}-^1\text{H}$  spin pairs. The absence of such couplings is consistent with the high mobilities of the mesostructure-directing P123 species within the hexagonally mesostructured silica channels under ambient temperature conditions. On the basis of the results in Figure 4 alone, however, no preferential interactions between the silica network and the different copolymer blocks can be distinguished. Selective interactions, typically with the hydrophilic PEO blocks, are presumed to be necessary for coassembly of the silica precursor species into the highly ordered mesostructured product materials.

At lower temperatures, however, molecular mobilities of the triblock-copolymer components can be reduced to allow preferential interactions with the inorganic framework to be elucidated. For example, the high surfactant mobility observed at room temperature is significantly diminished at approximately 260 K, allowing new intensity correlations to appear in 2D  $^{29}\text{Si}\{^1\text{H}\}$  HETCOR spectra. Specifically, the 2D  $^{29}\text{Si}\{^1\text{H}\}$  HETCOR spectra shown in Figure 5 acquired at approximately 260 K and two different contact times show strong intensity correlations that confirm interac-

tions between the different triblock copolymer moieties and the silica framework. 1D  $^{29}\text{Si}\{^1\text{H}\}$  CP-MAS spectra accompany each 2D spectrum along their respective horizontal  $^{29}\text{Si}$  axes, both of which show the same, but less resolved,  $Q^2$ ,  $Q^3$ , and  $Q^4$   $^{29}\text{Si}$  signals as observed at room temperature [Figure 4b] at  $-91.6$ ,  $-101.3$ , and  $-110.3$  ppm, respectively. At the longer 6 ms contact time [Figure 5a], weaker  $^{29}\text{Si}-^1\text{H}$  couplings contribute to greater  $Q^4$   $^{29}\text{Si}$  signal intensity at  $-110.3$  ppm, compared to the spectrum acquired with a short contact time of 1 ms [Figure 5b]. The single-pulse  $^1\text{H}$  MAS spectrum acquired at 260 K, displayed along the vertical  $^1\text{H}$  axis on the right of Figure 5b, shows broadened but resolved  $^1\text{H}$  peaks at 0.9 and 3.3 ppm, corresponding to the methyl-group PPO protons and overlapping signals from the  $-\text{OCH}_2-$  and  $-\text{OCH}-$  groups associated with the PEO and PPO blocks. The 2D  $^{29}\text{Si}\{^1\text{H}\}$  HETCOR spectrum in Figure 5a shows that both of these proton signals share strong intensity correlations with the  $Q^2$ ,  $Q^3$ , and  $Q^4$  moieties at  $-91.6$ ,  $-101.3$ , and  $-110.3$  ppm in the  $^{29}\text{Si}$  dimension, indicating strong interactions between framework silica sites and the mesostructure-directing P123 species at 260 K. This is in marked contrast to the 2D  $^{29}\text{Si}\{^1\text{H}\}$  HETCOR spectrum in Figure 4b for the same sample acquired at room temperature, which shows no 2D intensity correlations at 0.9 or 3.3 ppm in the  $^1\text{H}$  dimension and which are thus now clearly determined to be due to the high molecular mobilities of the P123 species at ambient temperature. For shorter contact times [Figure 5b, 1 ms] at 260 K, strong correlated intensity remains between the proton signal at 3.4 ppm and the  $Q^3$

(55) Engelhardt, G.; Michel, D. *High-Resolution Solid-State NMR of Silicates and Zeolites*; John Wiley & Sons: New York, 1987; pp 114–116.

and  $Q^4$   $^{29}\text{Si}$  signals at  $-101.3$  and  $-110.3$  ppm (and to a lesser extent the  $Q^2$  species at  $-91.6$  ppm), while significantly weaker correlated intensity is observed between these  $^{29}\text{Si}$  signals and the methyl PPO  $^1\text{H}$  signal near  $0.9$  ppm.

Intensity correlations also persist at low temperature between water proton signals near  $6$  ppm and those from the  $^{29}\text{Si}$  framework sites in both parts a and b of Figure 5. The different relative intensities of the 2D correlations for the different contact times can be more clearly seen in the projections onto the respective  $^1\text{H}$  axes for the two HETCOR spectra; in particular, the projected  $-\text{CH}_3$   $^1\text{H}$  signal near  $0.9$  ppm is much weaker relative to the  $-\text{OCH}_2-/-\text{OCH}-$  signals at approximately  $3.4$  ppm for the short  $1$  ms contact time, compared to that measured at  $6$  ms. These results, thus, establish that the PEO blocks of P123 interact more strongly than the PPO moieties with the mesostructured silica framework at  $260$  K, while at room temperature both blocks are mobile and weakly interacting (if at all) in the final THF-derived product. This is in contrast to ethanolic or aqueous syntheses, where a significant fraction of the PEO moieties remain occluded within and/or interact strongly with the silica framework, even at room temperature.<sup>54b</sup> This is also consistent with the different relative rates of silica cross-linking in these solvents (THF < ethanol < water)<sup>56</sup> and the relative miscibilities of the P123 blocks (water < ethanol < THF), which allow the blocks to be extracted from the silica walls, while remaining within the mesochannels.

The combination of the temperature- and composition-dependent interfacial structures and species dynamics revealed by solid-state NMR, together with the thermodynamic guidance provided by the ternary phase diagram, yield new molecular-level insights on the phase behaviors and transient processes that are responsible for the self-assembly of mesostructured silica-surfactant from THF-water solutions. The above results indicate that self-organization of the structure-directing P123 block copolymer species in a THF sol requires the availability of water molecules to form micellar or liquid-crystal-like phases. The presence of water, however, reduces the solubility of any highly hydrophobic guests (see below) in the solution, thus making it necessary to balance the water concentration in the synthesis mixture to enable surfactant self-organization and, at the same time, prevent the precipitation of highly hydrophobic guest molecules. This is achieved in the present study by gradually introducing water molecules to an initially nonaqueous (<2%  $\text{H}_2\text{O}$ ) THF solution containing dissolved P123, hydrophobic guest species, and hydrolyzed silica precursors. As the THF rapidly evaporates during the dip-coating process, the solution increases in viscosity and the remaining components become more concentrated. This promotes self-assembly of the P123 triblock copolymer species and also reduces the pH of the mixture. The decrease in pH accelerates condensation and cross-linking of the silica precursor species, releasing one  $\text{H}_2\text{O}$  molecule for each  $\text{Si}-\text{O}-\text{Si}$  bond that is formed. Under these conditions, the water molecules required to induce P123 self-organization are progressively generated in situ. The concentration of water molecules thus gradually

increases as the THF evaporates and the silica condenses. The water molecules present are expected to preferentially associate with the hydrophilic PEO blocks of the structure-directing P123 species and thereby promote the formation of micelles (Figure 1a), which subsequently self-organize further into highly ordered liquid-crystal-like mesophases. It is interesting to consider whether the micelles initially formed in THF are inverted, with PEO cores and PPO coronas. This would require, however, that such initially reversed micelles would apparently need to rearrange as the THF rapidly evaporates, to yield conditions where noninverted silica mesophase products result to be consistent with the 2D  $^{29}\text{Si}\{^1\text{H}\}$  HETCOR spectrum in Figure 5b. The NMR results show that the mesostructured silica ultimately formed has a hexagonal  $H_1$ -like structure with PPO cores and PEO coronas. The reduced rate of silica cross-linking in THF compared to in ethanolic solutions enables the P123 molecules, particularly the PEO moieties, to effectively extricate themselves from the cross-linking silica network before it fully solidifies.

**Incorporation of Conjugated Polymers during Syntheses of Mesostructured Silica.** The usefulness of processing mesostructured silica films from THF-water solutions is demonstrated by its efficacy for coassembling highly hydrophobic macromolecules, conjugated polymers in this case, into the hydrophobic regions of the mesostructured host during film formation. The conjugated polymer is introduced into the nonaqueous THF/P123/silica precursor solutions, which after dip-coating subsequently yielded mesostructured silica films, with the conjugated polymer species incorporated in the ordered hydrophobic PPO regions of the silica/P123 mesostructured composite. Two conjugated polymers were used in this study: orange-emitting MEH-PPV and blue-emitting PFO (see Experimental Section). These conjugated polymers were dissolved in THF and added to the THF-silica sol that was shown to yield either lamellar (1.0 TEOS:0.033 P123 molar ratio) or hexagonal (1.0 TEOS:0.017 P123 molar ratio) mesostructured silica. Addition of the conjugated polymer/THF solutions to the THF-silica sol resulted in clear colored precursor solutions, indicating that the conjugated polymers were dissolved and not present as colloidal aggregates. Dip-coating glass substrates into the precursor solutions produced thin translucent films with orange and blue/yellow tints for MEH-PPV- and PFO-incorporated mesostructured silica, respectively, revealing that the conjugated polymers were incorporated into the film during the dip-coating process.

Distinct reflections in the SAXS patterns of conjugated-polymer-containing films show that the dip-coating process resulted in the deposition of films with high degrees of mesostructural ordering. The SAXS patterns of PFO-incorporated silica films are similar to those obtained for films deposited from the same precursor solutions without conjugated polymer (Figure 3), as shown in the insets of Figure 6a,b for PFO-incorporated hexagonal and lamellar silica phases, respectively. The hexagonal PFO-incorporated film, Figure 6a, shows three reflections assigned to the  $\langle 100 \rangle$ ,  $\langle 010 \rangle$ , and  $\langle 110 \rangle$  planes with the channels aligned parallel to the substrate plane and a  $d$ -spacing of  $8.9$  nm for the  $\langle 100 \rangle$

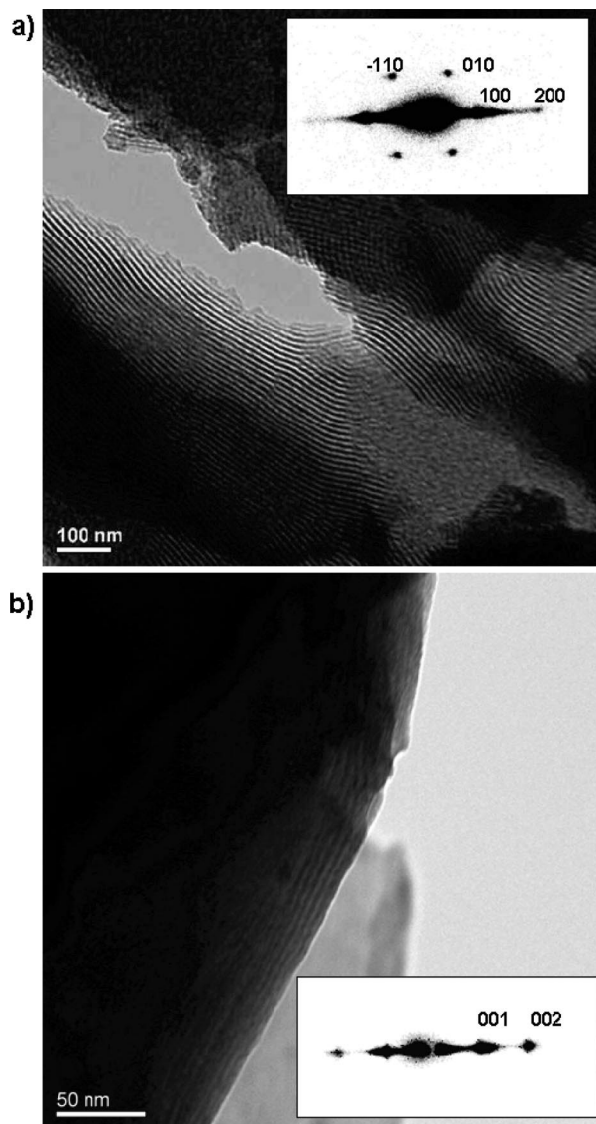


**Figure 6.** 2D SAXS patterns and TEM images of PFO-incorporated mesostructured silica films deposited from THF–silica precursor solutions with TEOS:P123 molar ratios of (a) 1:0.017 and (b) 1:0.033.

planes. A representative TEM image of the hexagonal PFO-incorporated film shows the cylinder arrays from the  $\langle 100 \rangle$  plane with a periodic spacing of 8.9 nm, in agreement with the SAXS measurement. The lamellar PFO-incorporated film, Figure 6b, shows two strong and exclusively out-of-the-film-plane reflections corresponding to  $d$ -spacings of 10.9 and 5.5 nm, respectively, and indexed as the  $\langle 001 \rangle$  and  $\langle 002 \rangle$  reflections of a lamellar structure aligned parallel to the substrate. The TEM image of the lamellar PFO-incorporated film in Figure 6b shows a diagonal cross-section of a lamellar silica domain, with periodic spacings of approximately 5 nm, about half the  $d$ -spacing determined by the SAXS measurement. 1D SAXS patterns (see Supporting Information) corroborate that PFO-incorporated mesostructured silica films have lamellar and hexagonal structures that are the same as for the films previously prepared from THF–silica sols in the absence of the conjugated polymer guest species. Such mesostructural ordering, furthermore, appears to be unaffected by the addition of the conjugated polymer species over a relatively large range of molecular weights, 50–500 kDa.

Interestingly, the incorporation of the conjugated polymers into the mesostructured hexagonal and lamellar silica films did not yield a significant increase in the  $d$ -spacing. Furthermore, the type of the incorporated polymer, glassy MEH-PPV<sup>57</sup> or rigid-rod PFO,<sup>58</sup> also did not affect the SAXS  $d$ -spacings. Two hypotheses could explain the absence of significant swelling upon conjugated polymer incorporation: (i) that the conjugated polymers are incorporated into the hydrophobic cores of the mesostructure but their concentration is either too low or their presence induces local disorder that is not readily detected by X-ray scattering or (ii) that the conjugated molecules are not incorporated into the mesostructured silica host but are macroscopically phase-separated as polymer aggregates distributed interstitially between mesostructured silica domains in the films. These two possibilities can be distinguished by analyzing the optical properties of the conjugated polymers in the composite film. The optical properties of conjugated polymers reflect the delocalization of  $\pi$ -electrons along their polymer chains and are therefore sensitive to the mean conjugation length of their polymer segments, their chain morphologies, and chain–chain interactions. Consequently, the optical absorption and emission spectra of the incorporated conjugated polymers can be used as sensitive probes to provide insight on the location(s) of the conjugated polymer species in the films.

The PL spectra of the conjugated-polymer-incorporated mesostructured silica films are generally similar to those of the corresponding pristine conjugated polymer films, as shown in Figure 7, indicating that the semiconducting polymer properties are maintained in the mesostructured silica. The PL spectra of MEH-PPV-incorporated silica and MEH-PPV pristine films in Figure 7a show a broad peak and shoulder centered at  $\sim 580$  nm and  $\sim 630$  nm, respectively. However, the incorporation of MEH-PPV into the mesostructured silica films, both lamellar and hexagonal, induces a noticeable  $\sim 10$  nm red-shift of the 0–0 vibronic transition peak (from 578 to 588 nm) and the shoulder (from 625 to 635 nm), compared to pristine polymer films (Figure 7a).<sup>57</sup> The red-shifted PL spectrum is consistent with a MEH-PPV chain morphology that is on average extended, compared to the pristine MEH-PPV film, due to confinement in the cylindrical mesostructured silica channels, which tend to favor extended polymer conformations and thus increased conjugation lengths.

The PL spectra of PFO-incorporated mesostructured silica and pristine PFO films in Figure 7b show three well-resolved peaks centered at 439, 467, and 498 nm, assigned to the 0–0, 0–1, and 0–2 vibronic transitions, respectively.<sup>58</sup> In contrast to MEH-PPV, the PL spectra of PFO-incorporated hexagonal and lamellar mesostructured silica films were *not* shifted to longer wavelengths, compared to the pristine PFO film. Extension of the mean conjugation length of PFO chains is apparently not induced by incorporation into mesostructured silica host matrices, probably because PFO has an intrinsically extended stiff rigid-rod morphology that is not appreciably affected by mesostructural confinement.

(57) Schwartz, B. J. *Annu. Rev. Phys. Chem.* **2003**, *54*, 141.

(58) Scherf, U.; List, E. J. W. *Adv. Mater.* **2002**, *14*, 477.

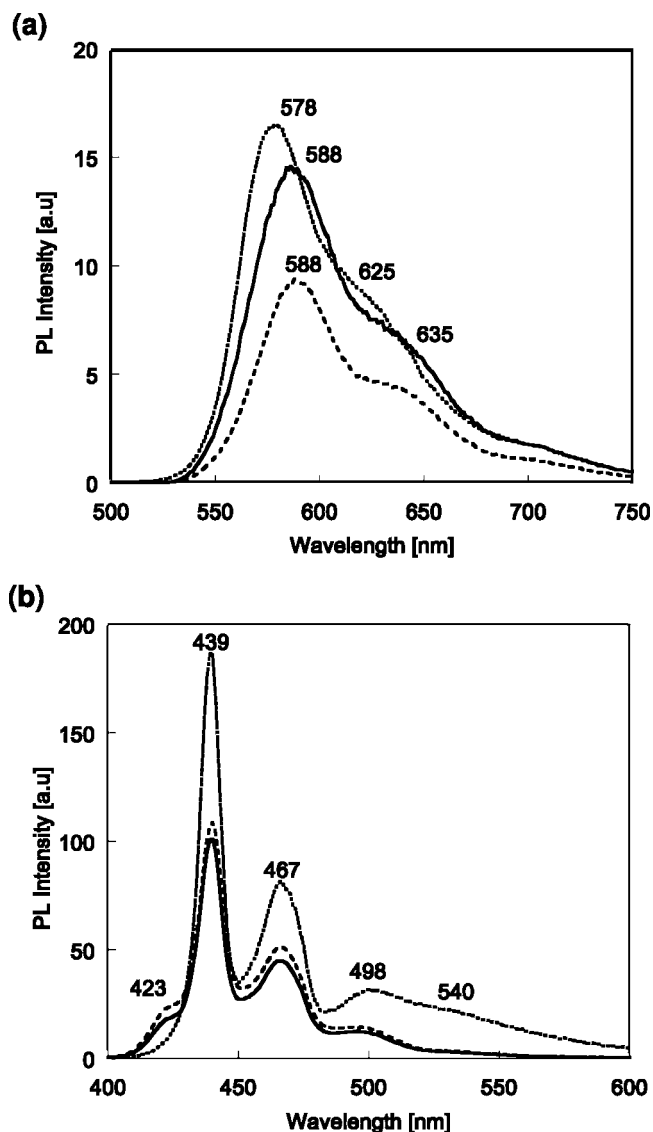


**Figure 7.** PL spectra of (a) MEH-PPV and (b) PFO conjugated polymer species as pristine polymer films (dotted lines), in lamellar mesostructured silica composite films (dashed lines) and in hexagonal mesostructured silica composite films (solid lines).

There are two differences in the PL spectra of PFO species in mesostructured silica and in pristine PFO films that also indicate distinct semiconducting polymer environments in the two films. First, as shown in Figure 7b for PFO in lamellar and hexagonal mesostructured silica films, a new shoulder is present at 423 nm, which is associated with the 420 nm peak observed in the PL spectra of PFO solutions, and is assigned to the 0–0 transition in disordered glassy ( $\alpha$  phase).<sup>59</sup> This is absent in the PL spectrum of the pristine PFO film, due to rapid energy transfer from the high-gap glassy phase to the low-gap extended phase, which are expected to be intimately commingled.<sup>58</sup> The appearance of this peak in the PL spectra of PFO-incorporated silica films indicates that encapsulation of conjugated polymer chains in host matrices can reduce energy transfer between confined chains, probably by reducing conjugated polymer chain–chain interactions through intermixing with PFO chains of the triblock copolymer species and isolation in the silica mesochannels. Inhibition of energy transfer between conjugated

polymer chains incorporated into an inorganic layered host was recently reported to yield white photo- and electroluminescence.<sup>60</sup> In addition, a second difference between the PL spectra of the pristine PFO and PFO-incorporated mesostructured silica film concerns the presence of a broad “green” peak at 540 nm in the former, which is not present in the latter. The band at 540 nm is associated with the presence of keto-defects on the PFO backbone, which have been shown to arise from oxidative degradation of the PFO chains.<sup>61</sup> The absence of this peak in the PL spectra of mesostructured-silica-incorporated PFO chains indicates that encapsulation in the silica films apparently protects the PFO chains against oxidation under otherwise identical film deposition and subsequent storage conditions.

More stringent tests and comparisons of environmental stability under harsher conditions provide additional evidence that the PFO chains are incorporated into the mesostructured silica host matrix and not present as macroscopically phase-separated polymer aggregates. Specifically, both lamellar mesostructured silica and pristine PFO films were immersed in vigorously stirred chloroform (an excellent PFO solvent) under ambient conditions for up to 4 days. Prior to rinsing, both films were annealed at 343 K for 3 h to promote cross-linking and stabilization of the silica network and to desorb solvent molecules (the normal boiling point of THF is 339 K),<sup>62–64</sup> without degrading the conjugated polymer guest species, which are stable to 703 K.<sup>65</sup> Annealing improves film durability, due to increased cross-linking of the silica, and results in modest reorganization the polymer chains, as evident from the absence of the glassy phase peak (420 nm) in the PL spectrum of the annealed film shown in Figure 8. The PL spectra in Figure 8 of the annealed PFO-incorporated lamellar silica film show that the PL peak intensities decrease by factors of two and five after 1 h and 4 days of immersion, respectively, in chloroform at 295 K, probably due to removal of PFO chains adsorbed on the external film surface and partial extraction of the PFO from the silica matrix. In contrast, immersing an annealed pristine PFO film in chloroform under the same conditions for only 5 min results in a reduction of the PL intensity by a factor of 200 (Figure 8, inset), indicating nearly complete removal of the PFO film. The preservation of the well-resolved vibronic features in the PL spectra of the mesostructure-incorporated PFO chains indicates that the chain morphologies are generally unaffected by extended immersion in chloroform.

Collectively, the PL results establish that significant fractions of the conjugated polymer species are confined in the mesostructured silica host matrices and not macroscopi-

(59) Winokur, M. J.; Slinker, J.; Huber, D. L. *Phys. Rev. B: Condens. Matter* **2003**, *67*, 184106.

(60) Aharon, E.; Kalina, M.; Frey, G. L. *J. Am. Chem. Soc.* **2006**, *128*, 15968.

(61) Sims, M.; Bradley, D. D. C.; Ariu, M.; Koeberg, M.; Asimakis, A.; Grell, M.; Lidzey, D. G. *Adv. Funct. Mater.* **2004**, *14*, 765.

(62) Feng, P.; Bu, X.; Pine, D. J. *Langmuir* **2000**, *16*, 5304.

(63) Crepaldi, E. L.; Soler-Illia, G. J. D. A.; Grosso, D.; Sanchez, M. *New J. Chem.* **2003**, *27*, 9.

(64) Gibaud, A.; Grosso, D.; Smarsly, B.; Baptiste, A.; Bardeau, J. F.; Babonneau, F.; Doshi, D. A.; Chen, Z.; Brinker, C. J.; Sanchez, C. J. *Phys. Chem. B* **2003**, *107*, 6114.

(65) Jun, L.; Changchun, M.; Quanguo, Z.; Yanxiang, C.; Lixiang, W.; Dongge, M.; Xiabin, J.; Fosong, W. *Appl. Phys. Lett.* **2006**, *88*, 083505.

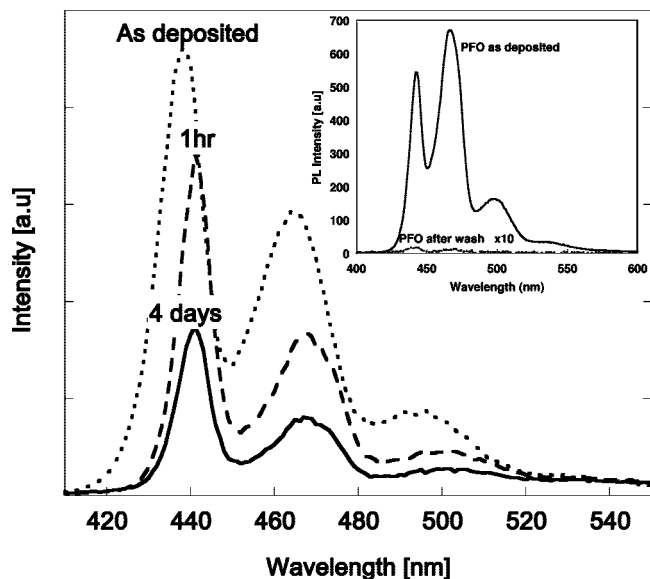


**Figure 8.** PL spectra of an annealed lamellar PFO-incorporated mesostructured silica film and after immersion in chloroform for 1 h or 4 days. Inset: PL spectrum of an annealed pristine PFO film and after immersion in chloroform for 5 min.

cally phase-separated as occluded polymer aggregates or adsorbed on the external film surfaces. The presence of some segregated domains of conjugated polymer in the films, however, cannot be excluded. The absence of significantly higher SAXS *d*-spacings upon incorporation of the conjugated polymers into both the hexagonal and the lamellar mesostructured silica films is likely due to their low conjugated-polymer loadings,  $\sim 1\%$  (see Experimental Section). Such low loadings also limit the use of 1D and 2D MAS NMR techniques for directly measuring the interfacial interactions and distributions of the confined conjugated polymers with respect to the structure-directing block-copolymer species and silica matrix, due to low signal sensitivity and/or low resolution.

### Conclusions

We have reported a new and general method for the syntheses of mesostructured silica films from isotropic solutions of network-forming silica precursors and structure-directing triblock-copolymer surfactant species, for example, Pluronic EO<sub>20</sub>PO<sub>70</sub>EO<sub>20</sub> (P123), in THF. As the THF evaporates during the dip-coating process, the silica condenses releasing one H<sub>2</sub>O molecule for each Si–O–Si bond formed. The gradually in-situ-generated water molecules associate preferentially with the hydrophilic PEO blocks of the surfactant, leading to P123 self-organization into liquid-crystal-like mesophases, similar to those observed in the ternary THF–water–P123 phase diagram. Silica cross-linking rigidifies the composite films into highly ordered hexagonal or lamellar mesophases, as identified by SAXS and TEM measurements.

The reduced rate of silica condensation in THF, compared to that in the aqueous solutions, permits the structure-directing block copolymer species to become extricated from the cross-linking silica before the matrix fully solidifies. Accordingly, <sup>13</sup>C NMR measurements show that the P123

copolymer blocks are highly mobile in the product film materials under ambient conditions, averaging dipolar couplings and accounting for the absence of 2D <sup>29</sup>Si{<sup>1</sup>H} HETCOR intensity correlations between the copolymer moieties and the silica network at room temperature. At lower temperatures (260 K), reduced mobilities of the copolymer blocks yield correlated <sup>29</sup>Si{<sup>1</sup>H} signal intensity in the 2D HETCOR spectrum between <sup>1</sup>H signals associated with the PEO blocks and <sup>29</sup>Si sites in the mesostructured silica framework. Such interactions are similar to mesostructured silica–P123 composites prepared from aqueous/ethanolic solutions, but differ in the much greater mobilities of the structure-directing block copolymer species in composites synthesized under more hydrophobic conditions.

The use of more hydrophobic synthesis conditions enables coassembly of highly hydrophobic guest species, such as conjugated polymers, during the formation of mesostructured silica host matrices. Silica-condensation-induced generation of dilute water molecules in initially isotropic THF–silica–P123 sols promotes P123 self-aggregation, with the dissolved hydrophobic guest species partitioning toward the hydrophobic PPO blocks. Evaporation of the THF during dip-coating causes liquid crystal-like mesophases to form, which are stabilized by high extents of silica cross-linking into mesostructured composites with the conjugated guest molecules incorporated into the hydrophobic PPO regions. PL measurements of MEH-PPV- or PFO-containing mesostructured silica films establish that significant fractions of the conjugated polymer species are confined in the silica mesochannels and not macroscopically phase-separated. This new hydrophobic approach is expected to be general and applicable to a variety of nonionic surfactants, inorganic host matrices, and especially highly hydrophobic functional guest molecules for tailoring the preparation of mesostructured inorganic–organic films with a wide range of optical, electrical, and structural properties.

**Acknowledgment.** This project was partially funded by the United States-Israel Binational Science Foundation, Grant 2002134. This work was supported in part by U.S. National Science Foundation under award DMR-02-33728 and the USARO-supported Institute for Collaborative Biotechnologies at UCSB. The NMR experiments were conducted using the Central Facilities of the UCSB Materials Research Laboratory supported by the MRSEC Program of the NSF under Award No. DMR 05-20415. S.C. and B.F.C. are grateful to Dr. Bénédicte Elena (Lyon, France) for pulse sequences and advice on NMR e-DUMBO homonuclear decoupling. C.R.-A. is grateful to the Ministerio de Ciencia y Tecnología (Spain) for support through the Ramon y Cajal program. B.F.C. was a 2006 Joseph Meyerhoff Visiting Professor at the Weizmann Institute of Science, Rehovot, Israel. The authors thank BASF for the donation of Pluronic P123 triblock copolymer.

**Supporting Information Available:** XRD patterns of PFO-containing silica films dip-coated from THF–silica precursor solutions (PDF). This material is available free of charge via the Internet at <http://pubs.acs.org>.